LCLS-TN-06-13

Transverse Coherence Properties of the LCLS X-ray Beam*

S. Reiche†, UCLA, Los Angeles, CA 90095, USA

October 31, 2006

Abstract

Self-amplifying spontaneous radiation free-electron lasers, such as the LCLS or the European X-FEL, rely on the incoherent, spontaneous radiation as the seed for the amplifying process. Though this method overcomes the need for an external seed source one drawback is the incoherence of the effective seed signal. The FEL process allows for a natural growth of the coherence because the radiation phase information is spread out within the bunch due to slippage and diffraction of the radiation field. However, at short wavelengths this spreading is not sufficient to achieve complete coherence. In this presentation we report on the results of numerical simulations of the LCLS X-ray FEL. From the obtained radiation field distribution the coherence properties are extracted to help to characterize the FEL as a light source.

1 Introduction

Self-Amplified Spontaneous Emission Free-Electron Lasers (SASE FEL) [1] allow to overcome the restriction in wavelength imposed by existing seeding sources and to explore new wavelength regimes. A particular interest is in the Ångstrom wavelength regime which opens entire new classes of experiments such the 3D imaging of individual molecules or the analysis of chemical reaction on the femtosecond scale. Supported by the successful demonstration of

*Work supported in part by the DOE Contract DE-AC02-76SF00515. This work was performed in support of the LCLS project at SLAC.

†reiche@ucla.edu

Table 1: LCLS Design Parameters

Beam Energy	13.4 GeV
Beam Current	3.4 kV
Undulator Period	3 cm
Undulator Parameter	3.5
Undulator Length	130 m
Radiation Wavelength	1.5 Å

SASE FELs at wavelength down to 14 nm [2], several X-ray FELs are currently under construction such as the Linac Coherent Light Source (LCLS) [3] or the European X-FEL [4].

The drawback of any SASE FEL is that it uses the spontaneous undulator radiation as its seed signal, which is intrinsically broadband and incoherent. Though the FEL process increases the longitudinal and transverse coherence by slippage and diffraction over the length of the undulator it never reaches the coherence level of a seeded FEL amplifier. In particular at short wavelength diffraction – the main method to the build-up transverse coherence – is ineffective and under certain circumstances the FEL can reach saturation before obtaining transverse coherence [5].

For the design of the optical transport line and diagnostic as well as proposed experiments it is of importance to characterize the radiation properties of the SASE FEL as a light source in advance. For that simulations were conducted and the results are presented here. The work was done in context of the LCLS (Tab.1 list the main parameters of LCLS). The main radiation properties have been presented elsewhere [6] and this presentation focusses solely on the fluctuation in the spot size at the detector locations (expressed by divergence and effective source location of the FEL beam) and the degree of coherence of the FEL signal.

2 Radiation Size and Divergence

Because a SASE FEL has no well-defined input to be amplified, the output is of stochastic nature and varies from shot to shot. For the purpose of designing the X-ray beamline the evolution of the FEL pulse along the optical beam line is of importance to know. In particular the divergence and beam size determine the design of apertures and target sizes.

The easiest quantities to extract from the results of FEL simulations are the rms sizes of the radiation pulse in the near and far field. To these values the envelope equation of a fundamental Gauss-Hermite mode [7]

$$w(z) = w_0 \sqrt{1 + \left(\frac{z - z_0}{z_r} \right)^2} \tag{1}$$

is matched. Although Eq. 1 has three unknown parameter – the waist size w_0, the waist position z_0 and Rayleigh length z_r – the system is fully deterministic because w_0 and z_r are related to each other by the radiation wavelength, which is a fixed parameter for our calculation.

Higher mode content obscures the results because the mode number becomes an additional unknown parameter. Due to the similarity of the Gauss-Hermite modes to the solution of the two-dimensional harmonic oscillator in quantum mechanics [8] and the fact that the calculation of the rms size is equivalent to the energy eigenvalue of the harmonic oscillator the waist size w_0 has to be corrected to $w_0 \rightarrow w_0(1+n+m)$, where n and m are the mode numbers of the Gauss-Hermite mode. In the far field zone ($z \ll z_0$) it can be also viewed as a reduction in the Rayleigh length $z_r \rightarrow z_r/(1+n+m)$ for a given and fixed waist size w_0.

The motivation for this work is to estimate the radiation size of the FEL pulse at any detector position in the far field zone. With that assumption we treat the entire higher-mode content as a single fundamental mode, defined by its Rayleigh length and waist position. This will yield wrong results at the source position by a mismatch in the actually waist size and the assumed one, however that information is irrelevant for the design process of the X-ray beam beamline and diagnostics.

As the initial step we analyze z_r and z_0 for the case of a seeded FEL with LCLS like parameters. The results are shown in Fig.1. The FEL is seeded with a radiation field ($z_r = 50$ m) larger than the electron beam size but after a few gain length the FEL-eigenmode is dominating. Because the mode size becomes smaller the Rayleigh length is reduced to about 20 m. In the lethargy regime of the FEL the radiation field remains almost unaffected and follows free-space diffraction as is seen by the almost constant waist position over the first 10 m. The FEL eigenmode has an intrinsic phase front curvature enhancing the diffraction and putting the source point behind the point where the field distribution is evaluated. At saturation gain-guiding vanishes and the phase front curvature straightens out as indicated by the growth in the Rayleigh length and a semi-constant waist position. However in deep saturation electrons gain some energy back while the radiation field has spread out by diffraction. This causes a disruption in the phase front at the electron location, coupling higher mode to the field distribution. As a result the diffraction is enhanced and the Rayleigh length becomes shorter.

SASE Simulations, using the LCLS design parameters, yield a radiation pulse with about 200 spikes at the undulator exit. Each spike is analyzed and the effective source position and Rayleigh length are extracted. To avoid that the analysis is obscured by the incoherent part of the radiation pulse (namely the area between spikes) only spikes are considered which have a peak power of at least 20 % of the maximum power in the pulse. Also we assume that over a single spike the phase fronts are very similar and thus can be treated as a single sample point.

As it can be expected from the intrinsic stochastic nature of the SASE FEL process there is fluctuation in both waist position and Rayleigh length. The

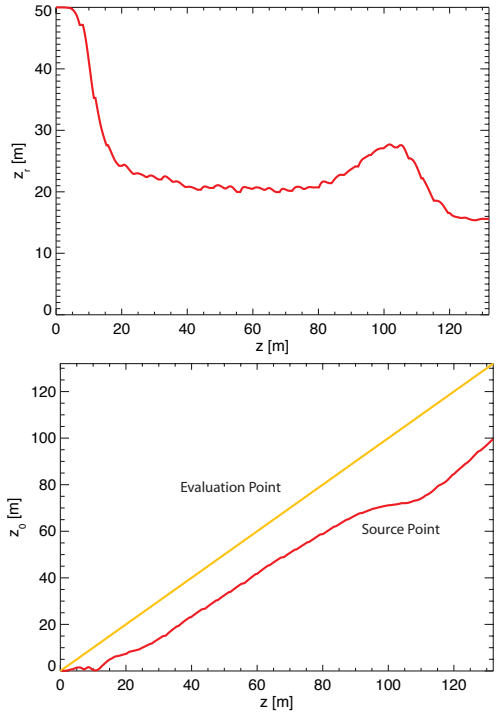

Figure 1: Effective Rayleigh length and waist position (top and bottom plot, respectively) along the undulator for an FEL amplifier.

distributions are shown in Fig. 2. The effective waist position is in average 38 m within the undulator from the undulator exit and has a rms fluctuation of 4.8 m. The average Rayleight length of 32 m is actually larger than the steady-state case. The rms variation is 4 m. The reason for a longer Rayleigh length is the deep saturation behavior of an SASE FEL, where the radiation further gains power in this super-radiant regime. The phase fronts are not as disrupted as in the seeded FEL case (see above). No significant correlation between Rayleight length and waist position has been observed.

Start-end simulations yield a different electron distribution than specified in the design case. Most notable is that only the electron bunch as a whole is aligned and match to the undulator axis while each slice has a certain degree of mismatch and misalignment. In addition wakefields are included which alter the energy of the electron along the undulator and thus disrupt the FEL process. While the statistic of the waist position remains almost unchanged ($< z_0 >=$ 37 m with an rms fluctuation of 5.7 m) the Rayleigh length is significantly shorter with 7.8 m and a rms variation of 2 m. Though some asymmetry in the electron distribution and the mismatch of the beta-function yield a coupling

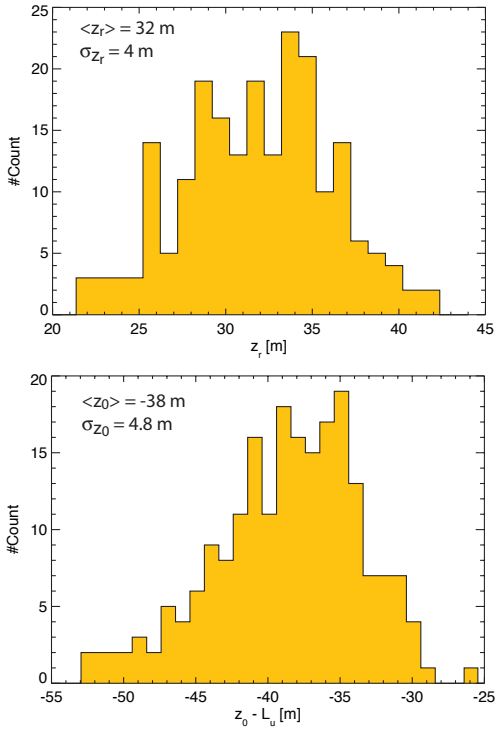

Figure 2: Histogram of Rayleigh length and waist position (top and bottom plot, respectively) for an SASE FEL pulse, evaluated at the undulator exit.

of higher modes to the emission the main reason is the centroid motion of the electron slices. In the saturation regime most electron slices undergo a turning point of their betatron oscillation. The strong focusing lattice provides a rather sawtooth-like trajectory, typical for any alternating-gradient focusing system, and the electron beam slice emits predominantly in two directions. Instead of once central distribution in the far field there are two overlapping distributions, left and right of the axis. The resulting distribution is significantly broader than for the aligned case, which is reflected by the shorter Rayleigh length in the statistic.

3 Coherence

In the previous section we expressed the quality of the SASE FEL radiation pulse by the fluctuation in the divergence and effected source position for all longitudinal modes (spikes in the radiation power profile). With the extracted Rayleigh length the size of a corresponding fundamental Gauss-Hermite can be

calculated and be compared to the radiation size of the FEL mode as an indication for the higher mode content. However higher modes are not necessarily an indication for poor transverse coherence. In the case that the phase relation between all modes remains constant from shot to shot corresponds actually to a fully transverse coherent pulse.

Coherence is a statistical property of a radiation source and refers to how much you can extrapolate the radiation phase information in time and space for any given measurement. Mathematically it is expressed by the mutual coherence function [9]:

$$\Gamma_{12}(\tau) = \left\langle \vec{E}(\vec{r}_1, t)\vec{E}(\vec{r}_2, t+\tau) \right\rangle \tag{2}$$

While the temporal coherence function is easy to define ($\Gamma_{11}(\tau)$) any experiment which relies on spatial coherence (e.g. diffraction on a grating) will always include some temporal information due to the difference in the path length to the detector. For sake of simplicity we assume that the signal $\vec{E}(\vec{r}, t)$ is quasi-monochromatic so that the time delay due to the path length difference from $\vec{r}_1$ and $\vec{r}_2$ falls within the temporal coherence of the signal and thus the time dependence in the mutual coherence function can be neglected. The mutual coherence function becomes then the mutual intensity $J_{12} \equiv \Gamma_{12}(0)$. In analogy to the temporal coherence function, the mutual intensity function is normalized as

$$\mu_{12} = \frac{J_{12}}{\sqrt{J_{11}J_{22}}} \tag{3}$$

to yield values between zero and one. It is referred to also as the complex coherence factor. A zero value refers to no correlation in phase between the observed field at the two postions $\vec{r}_1$ and $\vec{r}_2$ while a value of one means that the phase remains constant over time.

The complex coherence factor compares two fixed points in the transverse plane. If we allow both points to be free parameter μ_{12} would yield a four dimensional distribution. For sake of simplicity we restrict one point to be on the undulator axis. In analogy to the temporal coherence time [10] the coherence area is defined as

$$A_c = \int \mu_{12} dA \tag{4}$$

and reflects the size of a usable target area for experiments, relying on coherence, without the need to enforce coherence (e.g. with a pin hole). The optimum case would be when the coherence area is much larger than the actual spot size. Note that for a fully coherent signal the coherence area is infinite.

The entire field information of a time-dependent simulation for the LCLS design case was saved and used to evaluate the mutual intensity function and complex coherence factor. The resulting distribution for μ_{12} is shown in Fig. 3. The coherence area, as defined in Eq. 4, is 0.071 mm^2, about five times larger than the spot size Σ. This indicates sufficient transverse coherence over the entire spotsize and that the FEL pulse can be used for diffraction experiments without the requirement to enhance coherence by a pin hole aperture. The

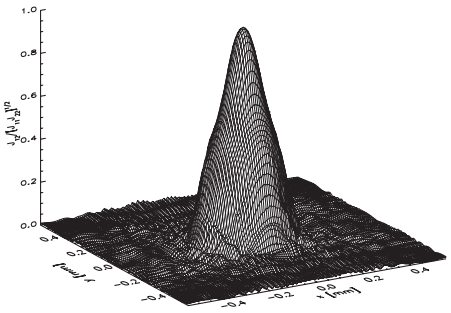

Figure 3: Complex coherence factor for LCLS design case at the undulator exit.

growth in the transverse coherence can be seen in Fig. 4 which is a monotonically increasing function along the undulator. On the other hand the radiation diffracts faster than the build up in the coherence area within the first tens of meter. However, at around 70 m gain guiding is dominant and the spotsize remains constant till saturation where the spot grows again due to diffraction. At around 60 m, the coherence area becomes larger than the spot size though it does not necessarily indicate good transverse coherence. For that the ratio between A_c and Σ must be much larger than one.

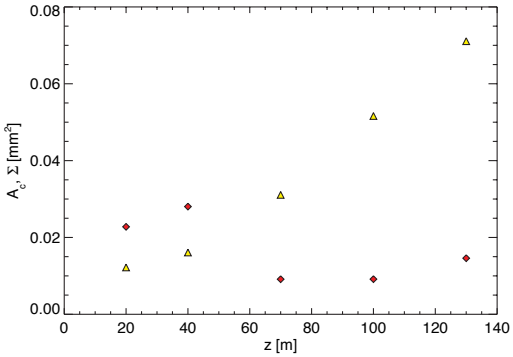

Figure 4: Evolution of the coherence area A_c and spotsize Σ (triangle and diamond shape, respectively) along the undulator.

For LCLS the FEL pulse has to propagate at least 115 m till it reaches the first user station. The coherence area is further increase and in the case of the LCLS design case the value becomes 0.32 mm^2 while the spot size is 0.044 mm^2. The reason is that noise consists typically of higher modes which diffracts stronger than the FEL pulse itself, clearing up the signal at the detector location. This becomes more apparent in the case of the start-end simulation where the electron beam slices are not aligned and matched to the focusing

lattice (see previous section). The complex coherence factor is shown in Fig. 5 and the resulting coherence area is 0.27 mm^2 while the spotsize is 0.057 mm^2. The ratio indicates that the coherence is still sufficient.

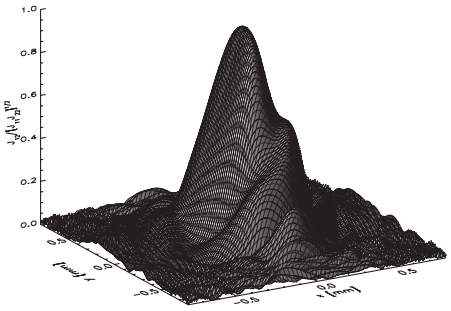

Figure 5: Complex coherence factor for LCLS for the start-end simulation, evaluated 115 m downstream of the undulator exit.

4 Conclusion and Outlook

Simulations have been conducted to study the radiation properties of the LCLS pulse, namely the variation in the beam size at the detector location and the degree of coherence. A fundamental Gauss-Hermite has been matched to each spike in the radiation profile to describe the divergence by an effective Rayleigh length and source position. The average source position is about 35 m within the undulator before the undulator exit and fluctuate by about 5 m. The Rayleigh length depends strongly on the underlying model of the simulation and shows significantly smaller values for start-end simulation. It is caused by centroid misalignment of the individual electron slice of the LCLS electron bunch. The build-up of transverse coherence during the FEL amplification process is sufficient to spread throughout the entire bunch. For the LCLS case The effective coherence area, within which the field amplitude and phase have a significant correlation to each other, is about 5 times larger than the spot size when evaluated at the first experimental location 115 m downstream the undulator.

The study will be continue to investigate toe major contributing factors to the widening of the divergence angle for the start-end case. Possible contributions are lower slice emittances, beam centroid mismatch, non-Gaussian beam distributions and deep-saturation behavior. The coherence properties will also be studied at longer wavelength, namely at a photon energy of 2 keV and 0.8 keV.

References

[1] R. Bonofacio *et al*, Opt. Comm. **50** (1984) 373

[2] A list can be found e.g. W.B. Colson, *Proc. of the FEL 2004 Conference* (2004) 706

[3] *LCLS CDR*, SLAC Report No. SLAC-R-593, 2002

[4] A.S. Schwarz, *Proc. of the FEL 2004 Conference* (2004) 85

[5] E.L. Saldin, E.A. Schneidmiller and M.V. Yurkov, Opt. Comm. **97** (1993) 272

[6] S. Reiche *et al*, Nucl. Inst. & Meth. **A483** (2002) 70

[7] A.E. Siegman, Lasers (University Science Book, Mill Valley, CA, 1986)

[8] S. Reiche, /it Numerical Studies for Single Pass HighGain Free-Electron Laser, Ph. D. Thesis, DESY report: DESY-Thesis-2000-012 (2000)

[9] J. Goodman, Statistical Optics (John Wiley and Sons, New York, 1985)

[10] E.L. Saldin, E.A. Schneidmiller and M.V. Yurkov, Nucl. Inst. & Meth. **A407** (1998) 291